Analysis of the Pullout of Single Fibers from Low-Density Polyethylene

JIAN-XIN LI*

Department of Chemical Engineering & Applied Chemistry, University of Toronto, Toronto, Ontario, Canada M5S 1A4

SYNOPSIS

In the present work, a single-fiber pullout test was used to study the interface/interphase between various fibers and low-density polyethylene (LDPE) and between glass fibers and a range of other thermoplastic matrices. For well-bonded fibers, experimental evidence suggests the involvement of plastic deformation and strain-hardening prior to debonding and pullout. The interfacial shear strength was determined to be the ultimate shear strength of the matrix and was found to be insensitive to the fiber surface structure. A new theoretical model was developed to predict the relationship between the debonding force and the embedded length. The contribution of friction to the debonding force was found to be insignificant when compared with the contribution of plastic deformation. © 1994 John Wiley & Sons, Inc.

INTRODUCTION

The nonlinear, or plastic, behavior of composite materials is attracting more and more attention as our understanding evolves. This is particularly true with the advent of fiber-reinforced thermoplastics, which have much in common with fiber-reinforced metal. In many situations, they cannot be treated as brittle, elastic materials.

The ultimate mechanical properties of the interface/interphase in composite materials have been extensively studied.[1] Among the different methods developed to measure the interfacial shear strength, the single-fiber pullout test remains the simplest and the most direct. It has the potential to provide basic input data for the interpretation of other test results, if proper theoretical models can be developed to analyze the pullout results and to extrapolate the simple tests to more complex situations.

During a typical single-fiber pullout test, the interface debonds in shear. The debonding force equals the integral of the interfacial shear stress over the entire interface. The normal stress on the fiber surface may be reduced by the Poisson contraction of the fiber in the radial direction of the highly stressed fiber during pullout. This may facilitate the initiation and propagation of the interfacial cracks. At the same time, Poisson contraction reduces the contribution of friction during pullout. Although theoretical models have been proposed[2,3] to account for the contribution of friction to debonding force, they cannot be confirmed because direct experimental evidence supporting a significant contribution of friction to the debonding force is still not available. Furthermore, the models usually assume a brittle matrix and interphase, but in many cases, experimental evidence supports plastic deformation and ductile failure.[4-6]

The lack of direct experimental support for model assumptions involved in the existing theories and the characteristic large scatter of experimental data allow the existence of conflicting theories. This conflict is further complicated by the difficulty in quantifying the interaction of the Poisson effect, adhesive strength, friction, and the debonding process.

In the present article, a new theoretical model was developed to predict the maximum pullout load for single fibers embedded in LDPE. The new model has been compared with some existing models, and

* Present address: Faculty of Pharmacy, University of Toronto, Toronto, Ontario, Canada M5S 2S2.

Journal of Applied Polymer Science, Vol. 53, 225–237 (1994)
 CCC 0021-8995/94/020225-13

new interpretations of the experimental results for different material systems are given.

EXPERIMENTAL

Preparation of Specimens

Two types of specimens were prepared: With type A, a pellet of the polymer was melted to fill a silicone oil (DC-20)-coated cylindrical capsule with a depth of 4 mm and a diameter of 4.85 mm. With method B, the polymer was melted on the flat bottom surface of the capsule as a substrate to form a 1 mm-thick polymer layer.

A flat polymer surface was produced by pressing before the solidification of the polymer. Using a needle, a hole was indented in the middle of that polymer surface. A fiber, confined in a capillary tube and fixed with masking tape, was inserted into the hole and the position of the capillary was fixed with the help of an embedding assembly.[7]

The assembly was then put into a preheated, temperature-controlled oven. A vacuum was applied to protect the specimen from oxidation. The assembly was taken out of the oven when it reached a specified temperature and cooled on a cold metal plate. The fiber above the polymer surface was cut with scissors, leaving about 10 mm of fiber for pullout. The embedded length was determined with a reading microscope after the fiber was pulled out.

Pullout Test

Pullout was done at room temperature, with a small Instron tensile machine. The specimen was fixed inside a sample holder that was linked to the crosshead through a load cell, and the fiber was bonded with cyanoacrylate resin to a copper plate immediately below the sample holder. The copper plate was fixed on a stationary holder. The crosshead speed was 1 mm/min.

Single-fiber pullout tests were conducted for LDPE, HDPE, LLDPE, and nylon 12 matrices mainly with epoxy compatible E-glass fibers. Neat E-glass fibers (without sizing), rubber-compatible E-glass fibers, Kevlar fibers, and AS-4 carbon fibers with commercial sizing were also pulled from the LDPE matrix for comparison. Silicone oil was used to coat the interior of the container with a treatment temperature of 220°C for 0.5 h, and it was also used in some tests as a fiber surface treatment to investigate the role of interfacial bonding. The mechanical properties of the materials used are shown in Table I.

Table I Data Used for Calculation and Comparison[8,9]

Matrix	E (GPa)	σ_u	ν
LDPE	0.2	14	0.32
LLDPE	0.35	20	0.32
HDPE	1.00	25	0.32
Nylon-12	2.80	46	0.32
E-glass fiber	72	3400	0.22
Kevlar fiber	130	3600	0.33
AS-4 carbon	233	3500	0.25

RESULTS AND DISCUSSION

SEM Observation and the Role of Transcrystallinity

The surface of a typical pulled out E-glass fiber from LDPE is shown in Figure 1. There is an obvious sheath of polymer on the fiber surface. This evidence suggests that the failure does not occur at the fiber–matrix interface, where the highest interfacial shear stress exists, but instead suggests the existence of a weak layer somewhat removed from the interface, which may be associated with the nonuniform crystallization in the matrix bulk and the transcrystallinity in the interphase, or sizing interpenetrated LDPE.

The micrograph also shows evidence of a plastic failure mechanism because the polymer layer is deformed. Traditional pullout models such as those of Piggott[3] are based on brittle interfacial failure and are unlikely to describe the failure process in a thermoplastic matrix.

Although there is potential relevance of transcrystallinity to the overall properties of fiber-reinforced thermoplastics, the influence of transcrystallinity (which should be fiber-dependent due to the fiber topography) on interfacial shear strength is not significant as is judged by the interfacial shear strength results for glass, carbon, and Kevlar fibers shown later on.

When the interfacial strength is higher than the cohesive strength of the matrix, it is impossible to measure the shear strength at the interface using a pullout test. The adhesive strength between fiber and polymer must be greater than the measured value.

Typical Pullout Curve and Pullout Test Results

A typical pullout curve is shown in Figure 2 for an E-glass fiber embedded in LDPE. As the experiment

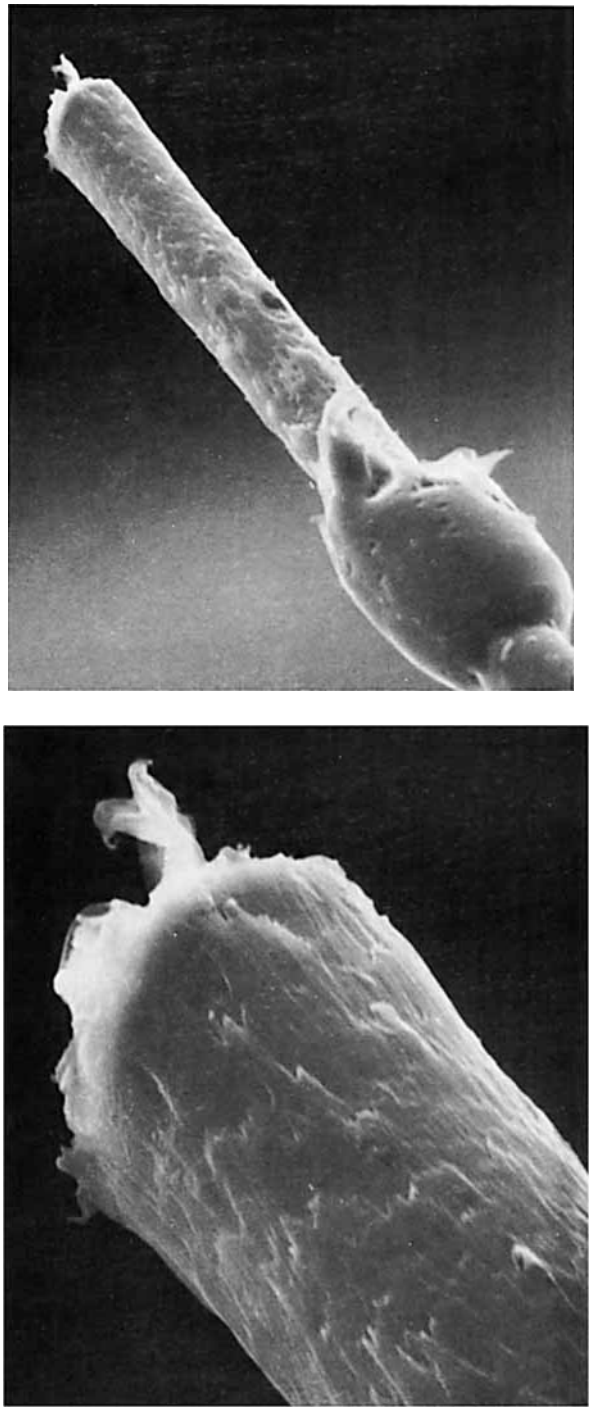

Figure 1 SEM photograph of the surface of a typical pulled out E-glass fiber from LDPE. The fiber has an epoxy-compatible sizing with a diameter of 22 μm.

starts, the load, F, increases linearly as the crosshead is displaced. This linear increase terminates, probably due to the onset of plastic deformation in the matrix. The load increases further, in a nonlinear manner, with displacement and reaches a maximum value F_a, the debonding force. This is followed by a drop in load to a much smaller value F_f, which is controlled by friction of the polymer against the moving fiber during withdrawal. The load gradually decreases to zero as the fiber is progressively withdrawn.

The averaged results for debonding force vs. embedded length for a series of tests are shown in Figure 3. The debonding force increases linearly with increases in the embedded length for small embedded lengths. This linear range is greater than what is predicted by the models based on brittle failure.[3] For longer embedded lengths, however, the debonding force increases nonlinearly with the embedded length. This implies that the failure is also not purely in a yielding mode.[3] It is probable that there exists a critical transition length, L_c, which determines the transition of failure from a plastically dominated pattern to a seemingly brittle pattern.

The apparent interfacial shear strength, $F_a/\pi dL$, is plotted against the embedded length, L, in Figure 4. This plot also provides evidence for the existence of a critical transition length, L_c. The apparent interfacial strength is constant for embedded lengths less than L_c. This suggests a uniform distribution of interfacial stress along the embedded fiber length for $L < L_c$. Since the interfacial shear strength is higher than the yield shear strength of the matrix, as evidenced by Figure 4, it is reasonable to propose that strain hardening is involved in the debonding process, as yielding does not always result in ultimate failure.

Figure 5 shows multiple peaks in the pullout curve for Kevlar/LDPE specimens. Because of the existence of defects and damage in the interphase,[10] the strain-hardened zone may become partially debonded at a lower load. This partial debonding would result in a detectable reduction of load because of the local release of the high interfacial shear stress. As will be shown later on, the value of L_c for Kevlar/LDPE may be reduced due to the high Poisson ratio of the Kevlar fiber. The length of the partially debonded region can also be very short for the same reason. It is conceivable that the local release of the high interfacial shear stress may not be significant enough to cause a high degree of instability to produce intermediate failure in the elastically stressed region. Further propagation of the interfacial crack could be prohibited by the plastic deformation of the interphase and more partial debonding may still be possible in the defect-rich zone before the final failure. The load could be built up again with the propagation of the strain-hardened zone. Once the

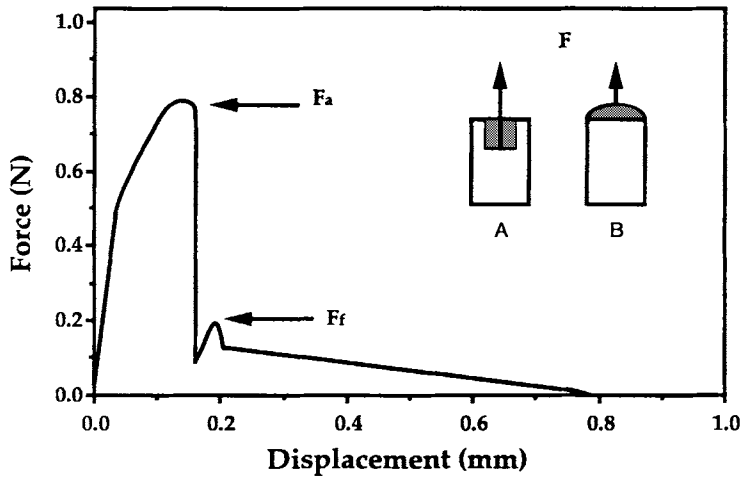

Figure 2 Typical pullout curve for E-glass fiber from LDPE.

critical length of the strain-hardened zone is reached, complete debonding will start if the tensile stress in the fiber is less than its tensile strength.

Theoretical Model

Basis

Based on the above discussion, the interfacial shear stress distribution along the fiber can be reasonably assumed to predict the effect of embedded length on the debonding force. The postulated stress distribution for fibers embedded more or less than the critical transition length is depicted in Figure 6. In this figure and in subsequent calculations, local stress distribution at the point of entry of the fiber into the matrix ($x = L$) and at the fiber end ($x = 0$) are ignored. Although these effects may be significant in initiating fast fracture in brittle matrix systems, they are unlikely to have a significant influence on the failure stress in the polyethylene matrix because of the presence of extensive yielding prior to failure.

In Figure 6(a), the evolution of the shear stress along the fiber for short embedded lengths is illustrated. This distribution is dependent on the ratio of Young's modulus for the fiber and matrix, E_f/E_m, and also on the aspect ratio of the fiber. For low loads, the stress distribution can be described by the elasticity equation of Cox[11] and would resem-

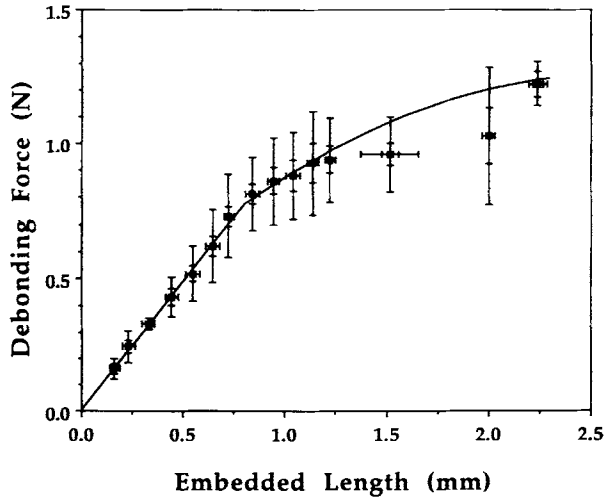

Figure 3 Average debonding force vs. embedded length for E-glass fiber (22 μm)/LDPE. Courtesy of Butterworth-Heinemann Ltd.

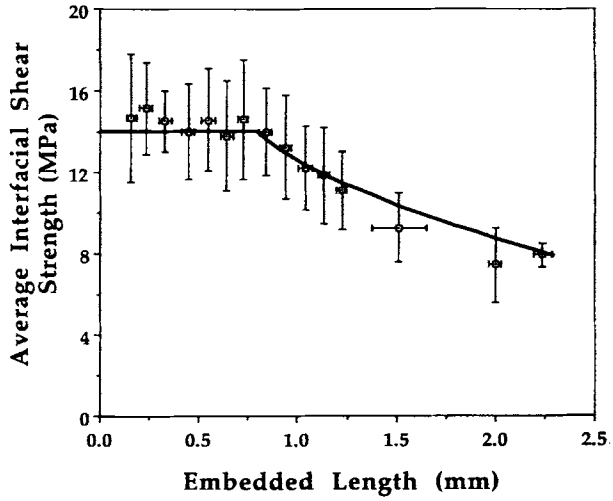

Figure 4 Apparent interfacial shear strength vs. embedded length for E-glass fiber/LDPE. Courtesy of Butterworth-Heinemann Ltd.

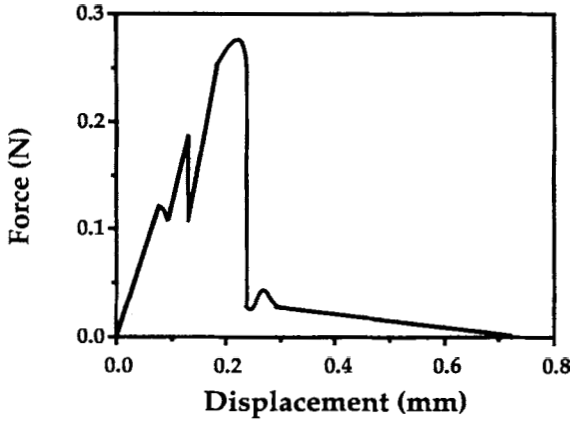

Figure 5 Typical pullout curve for Kevlar fiber from LDPE.

ble curves at the bottom. As the load increases, the maximum shear stress also increases, until the yield stress is reached near the matrix surface. It can be observed from the force displacement curve shown in Figure 2 that the onset of yielding causes a deviation from linearity, but does not immediately lead to failure.

As the load is increased further, the yield zone extends along the fiber and the material that yields first begins to strain harden. Failure is expected to occur when the maximum shear stress reaches the ultimate shear strength of the matrix. When this occurs, a relatively ductile crack propagates along the length of the fiber and the load decreases monotonically. The scanning electron micrographs (Fig. 1) show evidence of this ductile/tearing crack propagation, with small hackles of torn material bending toward the fiber end.

As has been shown by experiments, pullout tests for short embedded lengths can be adequately modeled by assuming that the shear stress along the entire embedded length is uniform and equal to the ultimate shear strength τ_{iu}. At some critical embedded length, L_c, the shear stress at the fiber end decreases sharply to the yield shear strength of the matrix. For embedded lengths greater than this, the matrix near the fiber end will not yield prior to failure, and this is depicted in Figure 6(b).

The maximum pullout force or debonding force, F_a, is equal to the integral of the interfacial shear stress over the entire embedded surface of the fiber at the onset of failure. It is clear from the discussion above that for embedded lengths shorter than L_c the failure load F_a would be approximately proportional to embedded length, since in this case, the surface shear stress is approximately τ_{iu} everywhere at failure. For embedded lengths greater than L_c, F_a is no longer proportional to embedded length, since part of the fiber is subjected to a shear stress that is less than the ultimate value for the matrix. This picture matches very well with the experimental data and is used as a basis for a simple quantitative model.

Mathematical Development of the Model

In the derivation of the model, it is necessary to make some simplification in order to reduce the

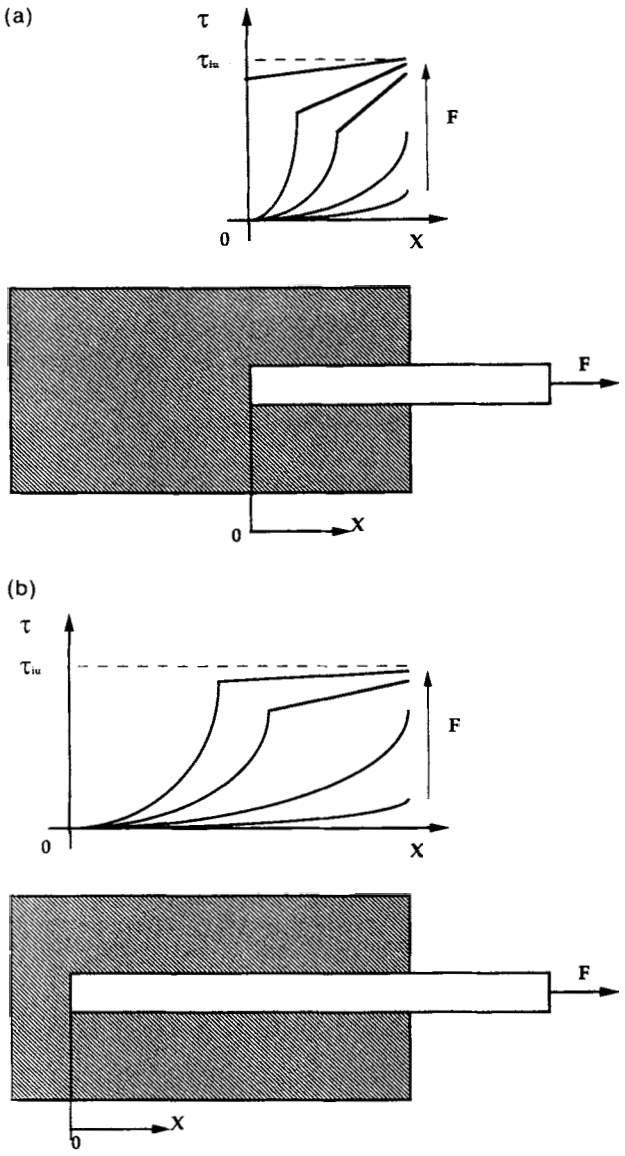

Figure 6 Postulated interfacial shear stress distribution: (a) embedded length shorter than the critical transition length; (b) embedded length longer than the critical transition length.

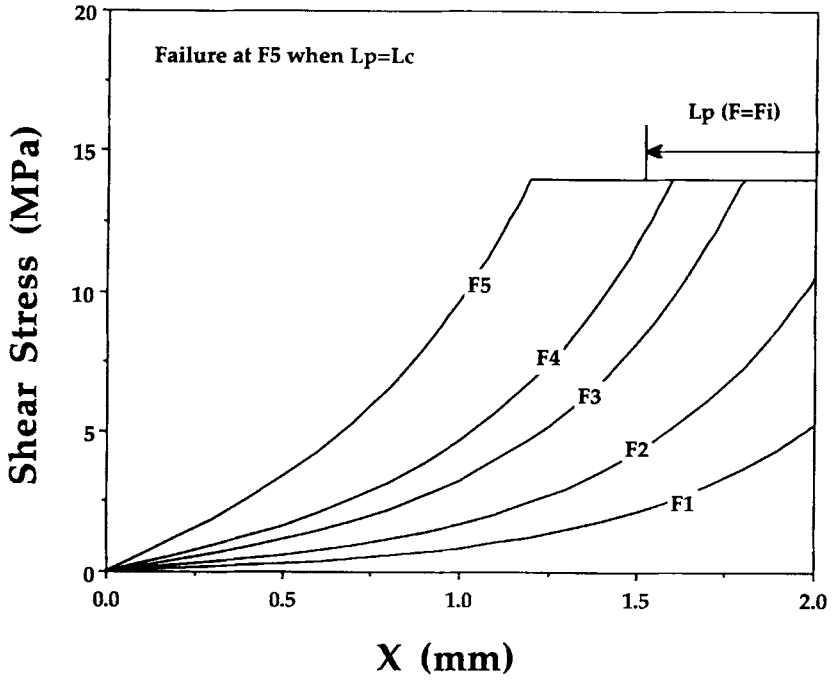

Figure 7 Simplified distribution of interfacial shear stress for modeling.

mathematical difficulties. A simplified picture of the stress distribution is given in Figure 7. In this model, the stress in the plastically deformed region is taken as a constant, equal to the ultimate shear strength of the matrix determined from pullout test with a short embedded length ($L < L_c$). This will be shown by the experimental data to be a very good approximation. Prior to yielding, the matrix will behave elastically, and the stress distribution is approximated by that given by Cox.[11] This simplification is acceptable only if the transition from elastic deformation to plastic deformation in the matrix takes place within a very narrow region compared with the total length of the plastic region (i.e., a sharp transition). The fiber is considered to deform elastically in all cases.

As discussed earlier, the cases of short and long fibers are very different and require different analysis. Hence, these two situations are analyzed separately.

Short Fibers $L \leq L_c$. The equilibrium of the interfacial shear force with tensile force in the fiber for an element of fiber with length dx requires

$$dF = \pi d\tau_i \, dx \tag{1}$$

The stress transfer at the fiber end is neglected, and if a uniformly distributed shear stress τ_i, close to the ultimate shear strength of the matrix, τ_{iu}, is assumed for the plastically deformed zone, then

$$F_a = \int_0^L \pi d\tau_{iu} \, dx = \pi d\tau_{iu} L \tag{2}$$

where L is the embedded length, and d, the diameter of the fiber. This leads to a linear relationship between F_a and L for small embedded lengths, which is consistent with the experimental results shown in Figures 3 and 4. Any substantial deviation of the surface shear stress distribution from the constant value τ_{iu} would lead to a nonlinear dependence of F_a on L, which would be inconsistent with the data.

Long Fibers, $L > L_c$. Equation (1) is also valid for this situation. When L_p is the plastically deformed length of matrix along the embedded fiber, the integral can be broken into two parts:

$$F = \int_{L-L_p}^{L} \pi d\tau_{iu} \, dx - \int_0^{L-L_p} \pi d\tau_i \, dx$$
$$= \pi d\tau_{iu} L_p + F_e = F_p + F_e \tag{3}$$

Cox's treatment[11] can be used to calculate the force due to elastic stress transfer, F_e. The shear stress at the fiber-matrix interface is related to the relative

displacement parallel to the interface by simple elasticity theory:

$$\tau_i = 2(u_f - u_m)G_m/\mathrm{d}\ln(D/\mathrm{d}) \quad (4)$$

where G_m is the shear modulus of the matrix; D, the diameter of the matrix surrounding the fiber; d, the fiber diameter; du_f, the displacement of the fiber in the axial direction at a distance x from the end; and u_m, the displacement of the matrix for the same x, a distance $D/2$ from the fiber axis. Equations (1) and (4) can be combined to obtain

$$dF_e/dx = \pi\mathrm{d}\tau_i = H(u_f - u_m) \quad (5)$$

where $H = 2\pi G_m/\ln(D/\mathrm{d})$. Since $du_f/dx = \varepsilon_1 = 4F_e/\pi\mathrm{d}^2E_f$, and $du_m/dx = \varepsilon_m$, Eq. (5) now becomes

$$d^2F_e/dx^2 = H(4F_e/\pi d^2E_f - \varepsilon_m) \quad (6)$$

The solution of Eq. (6) has the form

$$F_e = \tfrac{1}{4}\pi\mathrm{d}^2E_f\varepsilon_m + Q\sinh\beta x + S\cosh\beta x \quad (7)$$

where $\beta^2 = 4H/E_f\pi\mathrm{d}^2$, and Q and S are constants to be determined by the boundary conditions.

For the coordinate system shown in Figure 7, the equation describing the development of fiber force when $0 < L_p < L_c$ is obtained with boundary conditions

1. $x = 0, \tau = \tau_{\min}$
2. $x = L - L_p, \tau = \tau_{\max}$
3. $x = 0, F = 0$

we have

$$Q = -\pi\mathrm{d}\tau_{\min}/\beta$$

$$S = -\pi\mathrm{d}\tau_{\max}/\beta\sinh\beta(L - L_p) + \pi\mathrm{d}\tau_{\min}\coth\beta(L - L_p)/\beta$$

and

$$F_e = -S + Q\sinh\beta x + S\cosh\beta x \quad (8)$$

$$F_e = F_{\max}, \quad \text{when } x = L$$

$$F_{\max} = \pi\mathrm{d}L_p\tau_{\max} + \tfrac{1}{2}\pi\mathrm{d}\tanh\{\beta(L - L_p)/2\}(\tau_{\max} + \tau_{\min})/\beta \quad (9)$$

When $L_p = L_c$, $F_{\max}$ is the debonding force if the fiber stress $\sigma = 4F_{\max}/\pi\mathrm{d}^2$ is less than the fiber tensile strength. Otherwise, the fiber will have broken by this point. From FEM results,[12] it can be seen that although $\tau_{\min}$ is not identically zero it is small and can be set to zero for simplicity without significant influence on the theoretical prediction.

This treatment might also apply to single-fiber composite. It is possible that the calculation technique, frequently used by previous authors, might underestimate the interfacial shear strength for the single-fiber composite, since it is based on the assumption of a uniform interfacial shear stress distribution.

Comparison Between the Theories and the Experimental Results

Because of the large scatter of typical pullout data, various models may all be used to fit the data acceptably. Hence, the validity of a new theory cannot be judged solely by the quality of the fit. In this situation, the validity of the physical foundation of the theory must also be considered. The following is a summary of the other models of the pullout process that have been proposed. The comparison of models will be based on the data for epoxy compatible E-glass fiber/LDPE.

Yielding

For the process of failure by yielding, it is common to suppose the von Mises failure criterion to hold[3] and the yield shear strength to be the uniform shear stress over the entire embedded length prior to failure. This leads to the debonding force expression

$$F_{\max} = \pi\mathrm{d}L\sigma_y/\sqrt{3} \quad (10)$$

where L is the embedded length; d, the fiber diameter; and σ_y, the tensile yield strength.

Brittle Failure

If a well-bonded interphase fails in a brittle mode, both stress and energy criteria can be used to give an equivalent expression for the debonding force.[3]

$$F_{\max} = \tfrac{1}{2}\pi\mathrm{d}^2\tau_{\mathrm{iu}}\tanh(2nL/\mathrm{d})/n \quad (11)$$

$$n^2 = E_m/\{E_f(1 + \nu_m)\ln(D/\mathrm{d})\} = \frac{\mathrm{d}^2\beta^2}{4} \quad (12)$$

where τ_{iu} is the ultimate interfacial strength.

Brittle Failure with Partial Friction

If a well-bonded interphase fails in a brittle mode, and the friction in the partially debonded region contributes to the debonding force, the debonding force is expressed by[3]

$$F_{max} = \tfrac{1}{4}\pi d^2\{P/\nu_s - [P/\nu_s - 2\tau_d \tanh(ns')/n] \times (\exp(-2\nu_s \mu m s')\} \quad (13)$$

where $\tau_d = \tau_{iu}$, P is the radial stress on the fiber calculated based on the differences in thermal expansion,[13] μ is the frictional coefficient, m is the fraction of fiber debonded, and $\nu_s = \nu_f E_m/(1 + \nu_m)$ represents the fiber's Poisson effect.

Brittle Failure with Maximum Friction

In a physically unrealistic model, the friction in the whole interface is added to the force required for the brittle failure of the interphase. This gives the maximum debonding force for brittle failure involving friction:

$$F_{max} = \tfrac{1}{2}\pi d^2 \tau_{iu} \tanh(2nL/d)/n + \pi d L \tau_f \quad (14)$$

where τ_f is the frictional sliding stress. This provides a reliable upper limit for the maximum contribution of friction because it does not involve the uncertainties in the determination of Poisson's ratio and the confining stress.

New Model

The pullout force predicted by the new model presented in this work can be summarized as

$$F_{max} = \pi d L \tau_{iu}, \; L < L_c \quad (15)$$

$$F_{max} = \pi d L_c \tau_{iu} + \tfrac{1}{2}\pi d^2 \tau_{iu} \tanh(n(L - L_c)/d)/n, \; L > L_c \quad (16)$$

where L_c is the critical transition length for plastic deformation, which must be determined by a least-squares fit of the model to experimental results. To obtain Eq. (16), τ_{min} in Eq. (10) has been set to zero as a reasonable approximation, and τ_{max} has been taken as the ultimate shear strength of the polymer matrix, τ_{iu}.

Comparison with Experimental Results

Some of the parameters of the models involved in the comparison are not provided in Table I. τ_{iu} is currently estimated from the pullout results for $L < L_c$, which for LDPE was consistently found to be 14 MPa. σ_y is taken as 10 MPa.[9] The radial stress on the fiber, P, is estimated to be 2.24 MPa. The friction coefficient, μ, is assigned a value of 0.6, which is the highest value for slow sliding of LDPE against LDPE. The frictional sliding stress, τ_f, is taken as 2 MPa, determined from the sliding part of the pullout curve.

The comparison of the theoretical predictions of debonding stress vs. embedded length is shown in Figure 8. The experimental data are obtained from epoxy-compatible E-glass fiber/LDPE specimens, prepared with method A with the interior of the capsule coated with silicone oil. It may be concluded that the new model is in good agreement with the experimental results. In contrast, the contribution of friction is not sufficient to be concluded in the model to give good prediction as judged by the performance of the two models that assume a major contribution of friction. It should be noticed that with physically meaningful values of the selected parameters most of the other models do not give a good curve fit. The improvement of the prediction with the new model relies on the inclusion of the uniform stress zone that we attribute to the involvement of plastic deformation.

Evaluation of the New Model

To further validate the proposed model, it is necessary to vary the conditions in the pullout test and to examine the ability of the model to predict the results by fitting the data with Eqs. (15) and (16) and examining the resulting parameters, τ_{iu} and L_c to see if they vary in a physically meaningful way. Before describing these experiments, it is necessary to examine the values of τ_{iu} and L_c.

The scanning electron micrographs show that the failure is not a true interfacial failure, but rather a cohesive matrix failure very close to the interface. Therefore, the ultimate shear strength of the polymer will determine the ultimate interfacial shear strength. It is clear that the available value of τ_{iu} should depend only on the matrix material, unless the fiber surface treatment causes some substantial change in the structure of the adjacent polymer.

The physical interpretation of the parameter L_c and the subsequent prediction of how it should vary with the test parameter are much more complex. In physical terms, L_c is the length of the longest plastically deformed zone at the onset of catastrophic failure. Because the interfacial shear stress distribution also depends on fiber radius, L_c is expected to depend on the fiber radius.

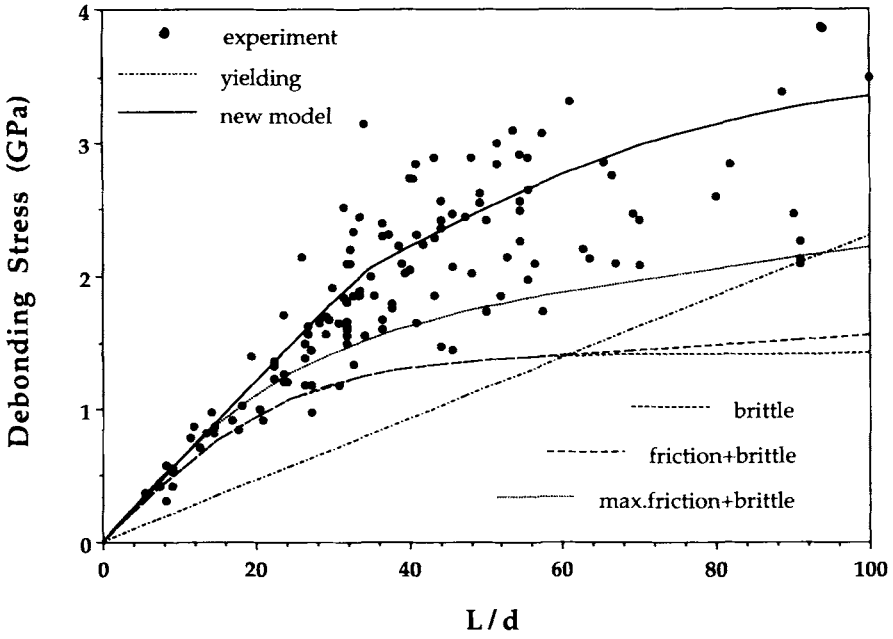

Figure 8 Comparison of the theoretical predictions of debonding stress vs. embedded length with the experimental result.

The Effect of Fiber Surface

The interfacial shear strength, τ_{iu}, is defined in eq. (17):

$$\tau_{iu} = F_a/\pi dL \qquad (17)$$

where the embedded length, L, already defined, must be less than L_c. For $L > L_c$, the nonuniform distribution of interfacial shear stress makes the calculation of τ_{iu} meaningless.

The results for neat E-glass fiber, rubber-compatible E-glass fiber, and epoxy-compatible E-glass fiber embedded in LDPE are summarized in Table II. The specimens were all prepared at 215°C with method A. Standard errors of the average values are used to indicate the confidence interval of the data.

The results for interfacial shear strength from the first three systems in Table II are about the same and agree reasonably well with recent measurement of the ultimate shear strength of LDPE based on a method recommended by ASTM.[14] These represent the situation in which the interphase is stronger than the matrix, so that the interfacial shear strength is determined by the ultimate shear strength of the matrix adjacent to the interphase. The results confirm the SEM observation that failure occurs in the matrix.

On the other hand, the pullout results for silicone oil-coated E-glass fiber represent the situation of very poor adhesion between the fiber and the polymer. In this case, failure occurs at the fiber–polymer interface, and the calculation of L_c using eq. (16) is clearly not applicable. With realistic parameters, equation (13) can be used to give a good fit of these data.

Effect of Fiber Diameter

The pullout results with neat E-glass fiber, rubber-compatible E-glass fiber, and epoxy-compatible E-glass fiber are shown in Figure 9. The Poisson's ratio is the same for all fibers in this situation. Although, theoretically, the fiber normal stress would be slightly higher for smaller fiber diameter, this difference could not be differentiated experimentally.

Table II The Pullout Results of Different E-Glass Fiber in LDPE

Fiber	Epoxy Compatible	Neat	Rubber Compatible	Silicone-coated
τ_{iu} (MPa)	14.0 ± 0.8	14.0 ± 0.9	15.0 ± 0.7	2.3 ± 0.2

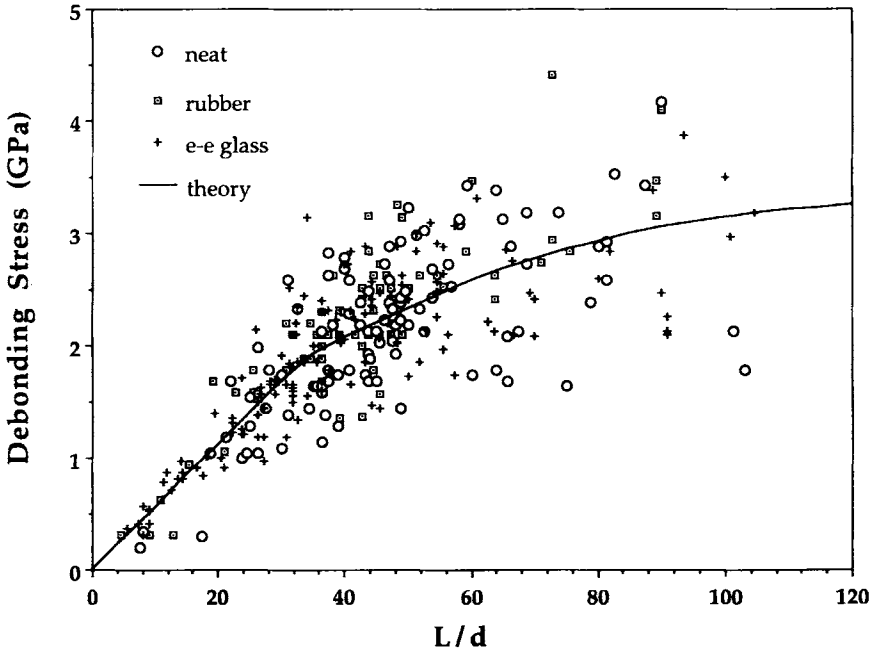

Figure 9 Pullout results for E-glass fiber with different diameters from LDPE.

The results of critical transition lengths for E-glass fiber with different radii are summarized in Table III.

In Table III, it can be seen that fibers with different diameters yield different critical transition lengths. However, the ratio of this length to the fiber diameter is approximately constant. This is consistent with the fact that stress distribution is mainly determined by the aspect ratio rather than the fiber diameter.

Effect of Fiber Modulus and Poisson Ratio

The pullout results for epoxy-compatible E-glass fiber, AS-4 carbon fiber, and Kevlar fiber with LDPE, prepared at 215°C, are summarized in Table IV. Again, the difference between the interfacial shear strength results for E-glass fiber and carbon fiber is not significant. The shear strength appears to be independent of the fiber properties. Although the result for Kevlar fibers is a little lower, the confidence intervals for the measured values overlap. Based on the present data, there is no basis to attribute any effect of fiber type on τ_{iu}.

The trend of the data for critical transition length for different fiber moduli is not consistent. This may be due to the variation in Poisson ratio between the different fiber types. This is expected to be another important parameter since, when the fiber is in tension, its diameter will be reduced according to the Poisson ratio effect and a tensile stress on the interface will be superimposed accordingly. This will reduce the residual stress on fiber and facilitate the damage or crack initiation process. Consistent with this, L_c would also be smaller. Also, because of the anisotropic character of the drawn fibers, the radial Young's modulus may be significantly different from the axial value used in the calculation. The radial Young's modulus may influence crack propagation. However, this modulus is extremely difficult to measure. Hence, this effect cannot easily be quantified.

Table III The Results for Different E-Glass Fiber in LDPE

Fiber	Epoxy Compatible	Neat	Rubber Compatible
L_c	0.74 mm	0.54 mm	0.39 mm
Fiber diameter (d)	22 μm	16 μm	11 μm
$S = L_c/d$	34	34	35

Table IV The Pullout Results for Different Fibers in LDPE

Fiber	E-glass	AS-4 Carbon	Kevlar
τ_{iu} (MPa)	13.4 ± 0.6	14.6 ± 0.9	13.2 ± 0.3
L_c	0.71 mm	0.23 mm	0.15 mm
Diameter (d)	22 μm	8 μm	16 μm
S	32	29	9
ν_{12}	0.22	0.25	0.33

As an organic fiber, the supermolecular structure of Kevlar fiber and, consequently, some of its properties might be changed upon exposure to an elevated temperature at 215°C. It might not be the best candidate for the comparisons in this work.

The Influence of Specimen Configuration

The pullout results from method A, with the internal wall of the capsule coated or not coated with silicone oil, and method B, with configurations indicated in Figure 2, are summarized in Table V. The fiber is an epoxy compatible E-glass fiber and the matrix is LDPE. The specimens were prepared at 215°C.

The sliding frictional stress, τ_f, is calculated as

$$\tau_f = F_f/\pi d L' \tag{18}$$

where F_f is the remaining force after the debonding, and L', the embedded length corresponding to F_f, may be estimated from the load displacement curve.

In Table V, it can be seen that the difference between the τ_{iu} determined by method A and method B is not significant. The reason for the consistency of the interfacial shear strength for specimens of different configuration, when the embedded length is less than the critical length, might be that the radial stress on the fiber, if there is any, is not high enough to cause significant change in ultimate strength.

However, the differences between the critical transition lengths in Table V are substantial. It is conceivable that boundary stress conditions in the radial direction may play a noticeable role in influencing the critical transition length and the debonding force, through its influence on the initiation of cracks. This is similar to the situation in which fibers with different Poisson ratios are embedded in LDPE.

With method B, the thermal deformation of the polymer layer is constrained by the rigid substrate that has a lower thermal expansion coefficient than that of the polymer. Consequently, compressive pressure on the fiber is reduced because the polymer cannot contract freely. This, when combined with the Poisson contraction during pullout, might facilitate the initiation of the crack and reduce the critical transition length and debonding force. This idea is also supported by the critical transition lengths determined for one group of the specimens prepared identically with method A except for the coating of release agent on the internal surface of the capsule. This is due to the fact that the presence of the tensile residual stress, which results from the adhesion between the polymer and the brass container wall, would also reduce the compressive pressure on fiber due to matrix shrinkage.

It seems that the specimens prepared with method A, when the interior of the capsules was coated with silicone oil, give untainted results for all embedded lengths. In these specimens, the matrix is free from external tensile constraint. This idea is also confirmed by τ_f for the coated capsule, which is higher than the rest due to the absence of the external confining stress (or boundary stress condition), which leads to an increase in the normal stress acting on the fiber. Based on the above discussion, it is apparent that meaningful comparisons can only be made for similar boundary stress conditions.

Pullout Test of Epoxy Compatible E-glass Fiber with Different Polymers and the Role of Friction

The results for LDPE, LLDPE, HDPE, and nylon 12 are summarized in Table VI. From the data in this table, it seems that S decreases with increase of the matrix modulus, E_m, or τ_{iu}. There is a distinct possibility that this effect could be caused by inadequate contact between the fiber and the high modulus matrices. Polymers of high stiffness usually have higher melting points and higher viscosity at the same temperature. These characteristics could lead to poorer fiber–matrix contact for a higher modulus matrix.

Table V The Pullout Results for Different Specimen Preparation Methods

Method of Preparation	A Coated	A Uncoated	B
τ_{iu} (MPa)	15.0 ± 0.8	15.1 ± 0.6	14.0 ± 0.5
τ_f (MPa)	2 ± 1	1 ± 1	1 ± 1
L_c (mm)	0.74	0.49	0.30
d (μm)	22	22	22
$S = L_c/d$	34	22	14

Table VI The Pullout Results for E-glass Fiber with Epoxy Compatible Sizing in Different Polymers

Material	LDPE	LLDPE	HDPE	Nylon 12
Temp of preparation	215°C	215°C	215°C	210°C
τ_{iu} (MPa)	13.4 ± 0.6	18 ± 1	23 ± 3	39 ± 2
L_c (mm)	0.71	0.46	0.35	0.22
d (μm)	22	22	22	22
S	32	21	16	10
E_m (GPa)	0.20	0.35	1.00	2.80
Melting point (°C)	108	125	130	175

The idea that the bonding is not dominated by friction can also be confirmed by a comparison of the interfacial shear strength results from LDPE and HDPE specimens prepared at 215°C given in Table VI. The normal stress on the fiber surface is about the same for LDPE and HDPE. Although the coefficient of friction for LDPE is lower than that of LDPE, the experimentally measured interfacial strength, τ_{iu}, for HDPE is still higher than that of LDPE. This is consistent with ultimate shear strength data of HDPE in the literature.[14,15] If good bonding is maintained, the interfacial shear strength of a ductile semicrystalline thermoplastic is controlled by its ultimate shear strength.

The Scatter of Data and Failure Mechanism

As is the case for most pullout studies, there is a large scatter in the pullout results. The results of the present work might provide some insight into the interfacial failure mechanisms that control pullout, based on the manner in which the scatter increases with embedded fiber length.

Penn and Chou[16] postulated that a defect might act as an initial crack within the interphase and that it could play a major role in the brittle failure of the interphase. For randomly sized and situated cracks, one would expect that the scatter of the data would reduce with increase in embedded length if an initial crack played a significant role. This is not reflected in the present experimental results for the material systems involved, since the absolute scatter seems to increase with increase in embedded length. This is further evidence that supports the hypothesis that the failure is not completely brittle.

The scatter of data might be partly caused by some initial defects at random positions with an irregular size distribution, due to the inadequate contact between the fiber and the matrix, along the interface, which reduce the true interfacial area and the debonding force. As a general rule, the longer the embedded length, the greater the possibility for the defect to be present, and therefore, the larger the scatter of the data should be.

The contribution of the naturally occurring inhomogeneity in the interphase due to the inherent local variation of the fiber surface energy may still play an important role as suggested by Penn and Lee.[17] The scatter of the data may reflect the nonuniform structure of the interphase produced. This scatter could be reduced in large-scale mechanical experiments.

CONCLUSIONS

The failure of the interface in the present material systems involves plastic deformation and cannot be reasonably described by the previous theories, using reasonable values of model parameters. A theoretical model was developed in an attempt to give a consistent interpretation of the pullout process. The model incorporates the concept of a critical transition length, L_c. For embedded length less than L_c, the pullout is adequately described by assuming a shear stress equal to the ultimate shear strength over the entire embedded length at failure. For fibers embedded more deeply than L_c, the model assumes a uniform shear stress, equal to the ultimate shear strength, over a length L_c of the fiber, and a shear stress that decays with position over the remainder of the fiber. Failure is precipitated by cohesive failure in the matrix that is initiated at the point where the fiber enters the matrix.

Direct determination of interfacial shear strength is feasible when the embedded length is less than the critical value. The interfacial shear strength has the value of ultimate shear strength of the matrix for well-bonded interfaces, regardless of fiber surface structure. The contribution of friction to debonding force is insignificant in this material system.

The author is grateful to Professor D. E. Cormack and Professor M. Kortschot for many valuable discussions and guidance during the preparation of the manuscript. He sincerely acknowledge Professor M. R. Piggott for his help during the initial stage of the research. This work was partially supported by DuPont (U.S.) and OCMR (Canada). Financial support through a University Open Fellowship is gratefully acknowledged.

REFERENCES

1. *Comp. Sci. Techn.*, **42**(1–3) (1991).
2. P. Lawrence, *J. Mater. Sci.*, **7**, 1 (1972).
3. M. R. Piggott, *Comp. Sci. Techn.*, **42**, 57 (1991).
4. M. R. Piggott and D. Andison, in *Proceedings of the American Society for Composites: 1st Technical Conference*, 1986, pp. 227–237.
5. P. Marshall and J. Price, *Composites*, **22**, 53 (1991).
6. N. Sato, T. Kauraucki, and S. Sato, *J. Mater. Sci.*, **19**, 1145 (1991).
7. M. R. Piggott and S. R. Dai, *Polym. Eng. Sci.*, **31**, 1246 (1991).
8. M. R. Piggott, *Load Bearing Fiber Composite*, Pergamon, Oxford, 1980, p. 89.
9. J. A. Brydson, *Plastics Materials*, p. 201. 4th ed., Butterworth, London, 1982.
10. L. S. Penn and S. M. Lee, *Fiber Sci. Tech.*, **17**, 91 (1982).
11. H. L. Cox, *Br. J. Appl. Phys.*, **3**, 72 (1952).
12. A. Hampe, private communication.
13. A. N. Aetravali, D. Stone, S. Ruoff, and L. T. T. Topoleski, *Comp. Sci. Techn.*, **34**, 289 (1989).
14. K. Liu, MASc Thesis, University of Toronto, 1992.
15. W. T. Mead and R. S. Porter, *J. Appl. Polym. Sci.*, **22**, 3249 (1978).
16. L. S. Penn and C. T. Chou, *J. Compos. Technol. Res.*, **12**, 164 (1990).
17. L. S. Penn and S. M. Lee, *J. Compos. Technol. Res.*, **11**, 23 (1989).

Received July 22, 1993
Accepted December 20, 1993